Proceedings of OMAE2005
24th International Conference on Offshore Mechanics and Arctic Engineering (OMAE 2005)
June 12-17, 2005, Halkidiki, Greece

OMAE2005-67077

EXPERIMENTAL AND NUMERICAL INVESTIGATION OF THE STABILIZING EFFECTS OF A WATER-ENTRAPMENT PLATE ON A DEEPWATER MINIMAL FLOATING PLATFORM

Christian A. Cermelli
Marine Innovation & Technology
Berkeley, California, USA

Dominique G. Roddier
Marine Innovation & Technology
Berkeley, California, USA

ABSTRACT

The stabilizing effects of a water-entrapment plate at the keel of a small three-legged semi-submersible platform are determined using laboratory experiments and time-domain simulations. Motion predictions were carried out in the time-domain using coupled-analysis between the vessel and its mooring, linear diffraction-radiation theory, and an empirical wave-viscous interaction model. Model tests were conducted at the U.C. Berkeley Ship Model Testing Facility to determine the validity of the numerical model.

INTRODUCTION

Exploration for oil and gas fields has been moving into deeper waters with a significant number of discoveries last year in water depth greater than 1,500 m in the Gulf of Mexico. With current technologies, only the largest fields can be produced because they contain enough hydrocarbons to justify the expenses of a deepwater production platform and associated pipeline infrastructure, or the smaller fields located within a few miles of an existing platform, as they can be tied-back to the existing platform.

New technologies in the area of subsea equipment, and improvements in surface technologies are aimed at reducing the threshold over which deep- and ultradeep-water fields can become economical. The MINIFLOAT platform is an un-manned minimal floating platform developed to provide a low cost support for surface equipment, and an interface between subsea equipment and a more distant production platform. The applications of this technology are described by the authors: Cermelli et al. (2004).

The platform is composed of three cylindrical columns with a rectangular section, and a large horizontal plate at the keel providing support to the columns, and covering the area between the columns, and extending around the columns as well; the model geometry can be seen in Fig 1. The water-entrapment plate is designed to shift the natural periods of the platform away from the wave energy, without providing a significant increase in displacement or without reducing the size of the columns. This large plate provides additional area for wave excitation, and at the same time additional damping due to vortex shedding along the edges of the plate.

Several investigators have researched the behavior of submerged horizontal plates: Prislin et al. (1998), Lake et al., (1999), however these were mainly concerned with added-mass and damping, because of the applicability to spars and the assumption that the plates were deeply submerged. In the present case, due to the limited draft of the platform, the plate is subjected to substantial wave excitation forces. Numerous researchers have worked on the problem of wave diffraction by various bodies. A comprehensive overview is provided by Newman (1977). In most instances, the assumption of inviscid potential flows is utilized. This pre-suppose that vortical features may exist and impact overall forces, but they can be treated separately using semi-empirical approaches, as they do not substantially affect the potential flow solution. The validity of this assumption in our case is questionable, and is the main topic of interest in this paper.

Another engineering application that includes significant viscous effects and wave interaction is the roll motion of a ship, particularly with bilge keels, which result in greatly increased viscous effects. Researchers have chosen to address this complex problem with Computational Fluid Dynamics, using RANS methods for instance, Chen et al. (2002) or vortex methods, Yeung et al. (2000). A simplifying assumption used in this case is that the main flow features are two-dimensional, hence the problem can be solved with sufficient accuracy by considering a two-dimensional “slice” of the flow. In the case of the three-legged column-stabilized platform investigated here, no such assumption can be made.

Laboratory testing of a small scale model of the platform were conducted at the U.C. Berkeley ship model testing facility. A description of the facility is provided herein. The challenges of testing a deepwater platform in a relatively small

 Copyright © 2005 by ASME

wave basin are exposed, and the methodology followed to address these issues is described in this paper.

A semi-empirical numerical model designed to predict the platform response was presented by the authors in 2004. Some of the parameters were adjusted based on present experimental results, and the performance of the model to predict platform motion is presented here.

EXPERIMENTAL PROCEDURE

The U.C. Berkeley ship model testing facility located at the Richmond Field Station, a few miles from the U.C. Berkeley campus, was selected for testing of the MINIFLOAT platform due to the proximity of this facility to the authors' offices, and also to its availability and flexibility. The main laboratory consists of a 200 foot long towing tank which is 8 feet wide and 5 feet deep. The tank is equipped with a hydraulic wave maker at one end, and a parabolic beach for wave absorption at the other end. A carriage spanning the tank, and capable of speeds of 3 knots is used for towing models.

The platform prototype is located in 6,000 feet of water in the Gulf of Mexico. It is moored with a 6 lines taut polyester mooring system. The response of the platform in realistic sea-states is the object of this work. A scale factor of 1/76 was selected as a compromise, allowing the extreme design event – a 35 foot significant wave height hurricane - to be generated approaching the limits of the wavemaker, and to obtain sufficient accuracy for lower operational sea-states.

The model, shown in Fig. 1a, is made of acrylic with some aluminum members supporting the deck. It weighs 26 lbs with ballast and instrumentation. A spreadsheet was developed to track all elements composing the model and compute mass properties. The mass matrix and location of center of gravity were adjusted by placing lead weights at the bottom of the columns and on the deck. The target metacentric height, GM, of 14 ft was confirmed by an incline experiment of the free-floating model performed by moving some of the ballast located on the deck. This yielded a GM of 14.5 ft.

The following instruments were placed on the model:

- six degrees of freedom accelerometer located on deck and providing linear and angular acceleration at the center of the deck;
- two resistance wave gages placed just outboard of column 1, and at the edge of the deck between column 2 and 3. These gages provide the relative wave elevation to help in determining the platform airgap;
- Three LEDs on stiff masts above the deck for the optical tracking system.

Tests were conducted in three headings: 0 deg, 90 deg, and 180 deg where the angle is the wave propagation direction relative to the model x-axis, as shown in Fig. 1b. Since the model geometry and mass properties are 120 degrees symmetric, the response of the platform in these three heading is sufficient to determine the platform response every 30 degrees, all around the platform.

Based on the selected scale factor and wave tank depth, the model water depth was only 380 ft, which is very different from the prototype depth of 6,000 ft. However, effects of the water depth are only felt through the response of the mooring system insofar as the deepwater wave assumption holds. Effects of the tank bottom on wave propagation are only felt for wave periods greater than 15 seconds in prototype scale. The effect of tank depth on the longer periods are shown to be small in a following section.

An equivalent mooring system was designed to provide the same restoring effects as the prototype for a given environment. The prototype mooring system is a 6 lines taut polyester system, and its response is linear over the entire useful range. The horizontal mooring stiffness could be matched by providing 3 mooring lines composed each, from the anchor, of a 4 foot long linear spring and a 1 foot long thin nylon rope connected to the fairlead on the model. The computed horizontal stiffness of the prototype and equivalent mooring systems are plotted in Fig 2a. The two stiffness curves are almost identical.

One of the factors to be considered in the design of the equivalent mooring system was the requirement to position the three anchors in all headings within the tank walls, which are only 8 feet apart. Consequently, the mooring line top angle was small with reference to the vertical axis. As a result of the selected configuration, a moment is applied to the platform by the equivalent mooring system as the platform offsets. The moment induced by the prototype mooring system on the platform as it offsets is very small. Fig 2b shows the results of a static offset test with a horizontal force applied at top of column 1, resulting in an overturning moment. In the prototype mooring case, the vessel rotation is due to the applied overturning moment, whereas in the equivalent mooring case, an additional rotation is caused by the effect of the surge on mooring line tensions. A 300 kips force applied at the top of column 1 results in a 3 degrees rotation with the prototype mooring system, and a 5 degrees rotation with the equivalent mooring system.

Wind and current typically contribute significantly to the response of a floating platform. They are usually modeled either with actual wind and current, generated by fans, and underwater nozzle or tank water recirculation, or with equivalent loads applied either statically or dynamically. Actual wind and current is sometimes perceived to be more realistic, but it introduces some uncertainties due mainly to turbulence, and scale effects. As a result, the value of controlled laboratory environment results is sometimes decreased as one tries to explain some unexpected responses by features of the wind or current generation system.

An alternative approach considered here, was to model the mean wind and current load by applying a constant horizontal force using low friction pulleys and weights. This model test practice is useful when the mooring response curve is nonlinear, and the proper mean offset must be imposed to achieve correct stiffness characteristics. In our case, the mooring stiffness curve is perfectly linear, and the equivalent mooring provides the same dynamic characteristics even if the offset is different. Therefore, tests were conducted with no additional mean load to model wind and current effects. This is not to say that wind and current effects are un-important. The present work that includes numerical and experimental work, is aimed at assessing the interactions of waves with the water entrapment plate. Wind effects can be superimposed to the wave exciting forces at the design stage to determine the response of the platform to a specified wind field. Wind coefficients may be obtained by numerical simulations using

Copyright © 2005 by ASME

wind blocks models, or by wind tunnel experiments. Currents effects are not as straightforward, as they may influence the magnitude of shedding from the edges of the water-entrapment plate. Model tests of the wave response with forward speed are considered to determine the current effects; however these could not be completed on time for this paper.

Wave reflections on the tank wall may generate inaccuracies in the experiment. However, these effects were relatively small for the following reasons: the parabolic beach design is very efficient for wave absorption. Series of regular waves generated by the wavemaker vanish almost completely as they move over the beach, and only very small reflected waves propagate back into the measuring area. In the case of regular wave tests, the test were run long enough to obtain a steady-state in platform response, but they were stopped before the energy of propagating regular wave had time to travel the length of the tank and back where the model was located.

Random wave tests were conducted to test the platform in realistic sea-states. These were one or three hour long in prototype scale (see test matrix presented in Table 1 below), which correspond to 8 or 22 minutes in model scale, and therefore sufficiently long that reflected waves will have time to travel back near the model. Calibration of the sea-states were conducted before the model was placed in the tank: several iterations of the wave maker transfer functions were performed in order to match the measured wave spectrum with the target one. During this process, wave reflection is present and it is expected to be similar to the cases with the model in place, and therefore the effects of reflection are considered to achieve the target wave spectrum. Some of the energy may correspond to wave components traveling back from the beach, and therefore the achieved spectrum is bi-directional, however, as stated above, reflection is small enough to minimize this problem.

Finally, because the tank is only 8 ft wide, waves diffracted by the model may reflect on the side walls and contaminate the platform response. Based, on the relatively small column size, with regard to wave length, diffracted waves are relatively small, and their reflection that reach the model are consequently not a source of significant inaccuracies.

A summary of the tests related to the performance of the platform in waves is provided in the table below.

Table 1: Laboratory tests matrix

	0 deg heading	90 deg heading	180 deg heading
Static offset	yes	no	yes
Decay	surge, heave, pitch	yaw	no
Regular waves	5 to 25 sec		
Random waves	Hs=10 ft, Tp=8 sec, 1 hour long Hs=15 ft, Tp=10 sec, 1 hour long Hs=35 ft, Tp=13 sec, 3 hour long		

NUMERICAL MODEL CALIBRATION

Numerical predictions of platform motion are conducted as follows: the vessel motion is obtained by solving Newton's equation of motion. It is assumed that the sea-state is relatively narrow-banded, and therefore the added-mass and damping coefficient only varies slightly within one standard deviation on each side of the wave spectrum peak. Although this approximation is not strictly necessary, it speeds up considerably the computations by removing the need to calculate a convolution of the vessel velocity and acceleration with the retardation functions. The resulting Newton's equation of motion reads as follows:

$$[m + m_a(T_p)]\ddot{\vec{x}} + [d(T_p)]\dot{\vec{x}} + [k]\vec{x} = \vec{F}_d + \vec{F}_m + \vec{F}_v + \vec{F}_w + \vec{F}_{sd} \quad (1)$$

where:

$[m]$ is the mass matrix

$[m_a(T_p)]$ is the added-mass matrix at the frequency of the sea-state spectral peak for heave, pitch and roll, and at the lowest frequency of the linear radiation solution for surge, sway, and yaw.

$[d(T_p)]$ is the wave damping matrix at the frequency of the sea-state spectral peak for heave, pitch and roll, and at the lowest frequency of the linear radiation solution for surge, sway, and yaw.

$\vec{x}$ is the 6DOF vessel response

$\vec{F}_d$ is the wave diffraction force

$\vec{F}_m$ is the mooring and tether force

$\vec{F}_v$ is the viscous forces on the column and on the plate

$\vec{F}_w$ is the dynamic wind force

$\vec{F}_{sd}$ is the slow-drift force obtained from linear calculations using Newman's approximation, Newman (1974).

Flow separation occurs downstream of the columns due to viscous interaction between the columns and the current and wave kinematics. As a result, additional loads, not computed by the linear diffraction-radiation theory are present. Morison equation is used to determine the viscous forces on the columns. Because the added-mass and wave inertia terms are accounted for in the diffraction-radiation solution, only the drag term is used. The columns are discretized in small viscous elements (line members, which are fixed with the body) on which the Morison equation is applied. The instantaneous location of the line members and wave kinematics at that location are calculated at every time step to determine the relative velocity between the body and the flow. The resulting viscous force is expressed as follows:

$$F_v = \frac{1}{2}\rho C_d DLU|U| \quad (2)$$

where $U = \mathbf{t} \times (\boldsymbol{u_C} + \boldsymbol{u_W} - \boldsymbol{u_B}) \times \mathbf{t}$ is a vector component in a plane normal to the axis of the member and in a plane defined by the relative velocity and the line member axis. **t** is a unit vector along the axis of the line member, and L is the length of the line member.

$\boldsymbol{u_C}$ is the current velocity, $\boldsymbol{u_W}$ is the wave-induced velocity based on linear superposition and the Wheeler stretching method, Wheeler (1969), and $\boldsymbol{u_B}$ is the body velocity at the location of the line member. Numerical simulation were conducted with C_d=1.2 on the columns. D is a characteristic dimension of the column taken to be 0.5($L1$ +$L2$) where $L1=44.3ft$ is the length of the long side of the column, and $L2=25.3ft$ is the length of the short side.

Flow separation also occurs along the edges of the water-entrapment plate. Similarly, viscous elements with a Morison model (equation 2) are generated along the edges of the water-entrapment plate. The resulting viscous force is assumed to be normal to the plate, and therefore:

Copyright © 2005 by ASME

$U = [(\boldsymbol{u}_C + \boldsymbol{u}_W - \boldsymbol{u}_B) \cdot \mathbf{n}]\mathbf{n}$ where $\mathbf{n}$ is a unit vector normal to the plate. The drag coefficients of various submerged horizontal plates have been measured by Prislin et al. (1998). They recommend a Cd value between 5 and 10 for a square plate when analyzing results of model tests. Some differences are expected here, because viscous effects from the plate will arise from motions of the plate as well as the kinematics of the waves. Furthermore, interactions may occur between vortex-shedding and potential flow affecting the combined loading on the plate.

The mooring system is solved using a finite-difference scheme, coupled with a time-marching algorithm to solve the Newton's equation of motion for the platform. More details on the numerical model are provided in an earlier paper by the authors: Cermelli et al. (2004).

The static offset test is the first test conducted in the wave basin after the model is ballasted, placed in the water and attached to its mooring. A horizontal force is applied to the model using calibrated weights suspended to a low friction sheave. A similar configuration is numerically determined. This serves to verify that the static behavior of the mooring is properly determined by the numerical model. The experimental data points plotted on Fig. 2a fall very close to the predicted horizontal stiffness of the equivalent mooring system.

The horizontal force was applied at the top of column 1 in order to generate an overturning moment as well. This part of the test serves to verify that the mooring moment due to surge and the hydrostatic pitch stiffness are as expected. The hydrostatic stiffness in pitch depends on the vessel displacement and longitudinal metacentric height GM_T. As shown in Figure 2b, the combination of the mooring moment and pitch hydrostatic stiffness are well predicted by the numerical model. As stated in a previous section, the prototype mooring response is somewhat different, because the moment due to the offset could be minimized significantly (approximately 10% of the moment generated by the equivalent mooring for a same offset).

Decay tests are then conducted to determine inertia and damping properties of the system. Results of these tests were used to determine the drag coefficients applicable to this particular model test conditions. It was assumed that damping from the mooring lines is fairly small because the mooring lines are short. The column drag coefficient was adjusted to match the surge decay response, as shown in Fig 3a. The column Cd was set to 3.0 based on the characteristic dimension D=0.5[$L1$ +$L2$] (average of long and short sides of column). Although this value is somewhat higher that what would be used for a full scale prototype (Cd of a rectangular section is closer to 2.0), the differences are due to the relatively small scale (Reynolds number) and Keulegan-Carpenter number.

No adjustment were made to modify the resonant period: stiffness properties were verified by the static offset test, mass was simply measured on a scale, and confirmed by calculation of the weight of each element composing the model. So the good agreement in period is an indication that the added-mass computed by the linear diffraction-radiation code WAMIT are well predicted.

Similarly, the heave decay test was used to determine Cd's to be used around the edges of the water-entrapment plate. The value of Cd used in computations shown in Fig 3b are 10.0 based on the overall heave force ratio over plate area. This is consistent with experimental results achieved by other investigators as detailed in the previous section. Mass or stiffness properties did not require tuning, again indicating that heave added-mass is well captured by WAMIT, which includes a dipole model on the water-entrapment plate.

Finally, results of the pitch decay tests are presented in Fig 3c, with no further calibration of Cd's in the numerical model. Again, the reasonable agreement between measured and calculated pitch confirms the proper computation of pitch added-moment of inertia.

RESULTS

The tests described in the previous section are meant to confirm the proper physical and numerical modeling of the mooring system, hydrostatic properties of the platform, mass and added-mass and damping effects. Once these elements are understood, the response of the platform in regular waves can be determined numerically provided the wave excitation forces, combination of Froude-Krylov and diffraction forces, are known.

Regular wave tests were performed for frequencies between 5 and 25 seconds. The Response Amplitude Operators (RAO's) are plotted in Figure 4a for the heave of the platform with 0 degree wave heading. The wave slope was 5% for the shorter period and decreased progressively near 1% for the longer period. The high frequency limit was such that the linear wave theory would still be valid, and the low frequency limit was set by the maximum wave maker stroke.

Comparing with the numerical base case (Cd x1) in which drag coefficients on the plate edges are based on decay test results, the heave RAO is slightly underpredicted in the frequency range [12-16 sec] and slightly overpredicted in the frequency range [17-22 sec]. The heave natural period is approximately 16.5 seconds. A sensitivity on the drag coefficient along the plate edges utilized in the viscous-wave interaction model was then conducted, by doubling, and halving the Cd's. The case with higher Cd's - corresponding to an overall Cd of 20 based on plate area – provides a very close match with the experimental results.

The pitch RAO at 0 degree wave heading (Fig. 4b) is similar to numerical predictions for periods up to 10 seconds, but oscillations of the numerical response for longer periods, which are due to tuning of the wave length with the hydrodynamic plate model, do not seem to be as pronounced in the experiment.

The surge response is shown in Fig. 4c. It is noted that significant drift was observed in the surge response, and a high-pass filter was applied to process the RAO from experimental data. The first order response follows the linear deepwater hydrodynamic results, indicating that the effects of waterdepth in the wave tank are small even for the longest wave periods.

Figure 4d presents the yaw RAO for waves at 90 deg heading. The yaw response at 0 degree heading is very small because of the symmetry. The maximum yaw response at 90 degrees occurs at a period close to 6 seconds, where the wave length results in out-of-phase loading on the three columns.

As noted above, regular wave tests are a way to assess the performance of a numerical model in predicting wave exciting forces, provided all the tests described in the previous section are performed carefully. Irregular waves, which are representative of actual sea-states that may impact the platform,

Copyright © 2005 by ASME

provide additional challenges: non-linear force components combine to provide excitation at periods much greater than the wave periods, exciting the platform natural frequencies in surge, sway and yaw. In addition, wave crests must clear the deck by a sufficient margin to prevent the possibility of severe structural damage during a storm.

The extreme event selected for this study is a hurricane with 35 foot significant wave height and 13.0 seconds peak period. Although the wave height is slightly smaller than that of a typical 100 year hurricane in the Gulf of Mexico (around 40 ft Hs), the peak period is shorter resulting in increased exposure of the platform to impact by wave crests: with a natural period in heave around 16 seconds, the MINIFLOAT platform is designed to heave significantly during a hurricane event. This behavior is used to reduce the deck height above the Mean Water Line by allowing the platform to "ride over the wave crests". The heave natural period can be tuned by modifying the size of the water-entrapment plate in order to achieve motion envelopes in hurricane that are consistent with the risers, umbilicals or electrical cables that must be suspended to the platform. As the natural period in heave increases, the deck height must be raised to accommodate the highest wave crest, resulting in a larger and costlier structure. The optimum depends on platform functionalities, and required payload as well as the performance of connected risers and umbilicals.

Figure 5a compares the target spectrum, a Jonswap spectrum with γ=3, with the experimental one. The measured Hs is within 5% of the target value. The distribution of the extreme wave crest during a 3-hour storm is plotted in Fig 5b together with a numerical model of expected wave crest based on Forristall second order crest model, Forristall (1999).

Spectral responses of the platform during the design event are provided in Figs 6a to 6c. The low-frequency surge (Fig 6a) at the surge natural period (110 seconds) is significantly underpredicted by the model, which includes second order effects due to the body moving in irregular waves, as well as nonlinear loading from the Morison model on the columns combined with the wave kinematics. The discrepancy is likely due to the run-up effects, which are neglected in the model, and can cause significant nonlinear forces on the columns due to nonlinear deflections of the free-surface around the columns. This effect is well described by Trulsen and Teigen (2002), who investigated the run-up on vertical cylinders using nonlinear potential flow models and experiments.

By arbitrarily increasing the slow-drift contribution (from Newman's approximation) by a factor of 3, a perfect match could be obtained in the low frequency surge response, indicating that the magnitude of run-up forces is twice that of the mean drift forces. No further attempts were made to improve the predictions by including an empirical wave run-up model.

The heave spectrum (Fig 6b) determined experimentally contains more energy that the time-domain predictions near the peak period (12-16 seconds), which is consistent with the RAO results of Fig 4a, since the time-domain predictions were conducted with the base case drag coefficients.

The pitch spectrum from numerical simulations, shown in Fig 6c, exhibits some waviness in the high frequency range due to a relatively low number of frequencies used to generate the Fourier series of incident waves. In the present simulations, 100 frequencies were used to discretize the specified wave spectrum. A simulation with 200 frequencies (not shown here) resulted in smaller oscillations. Similarly to the surge, the nonlinear pitch response at frequencies near the pitch resonance (25 seconds) is not predicted by the numerical model. The second-order pitch moment was included in the slow-drift calculations but these do not cause visible motion, probably because of the high damping level. Additional pitch moment due to run-up effects is probably what causes the response of the platform near the pitch resonance.

Table 2 below summarizes the responses of the platform in the design event.

Table 2: Extreme response in hurricane, experimental and numerical(in feet and degrees)

EXPERIMENTAL	mean,	rms,	max,	min,
wave	0.00	8.85	36.29	-34.23
surge	1.14	14.52	36.03	-59.65
heave	0.04	4.81	18.19	-18.82
pitch	0.03	1.95	10.03	-6.33

NUMERICAL	mean,	rms,	max,	min,
wave	0.00	8.61	32.55	-31.99
surge	-4.27	9.79	17.96	-58.20
heave	-0.20	4.07	14.44	-16.48
pitch	0.20	1.92	8.90	-8.17

The determination of airgap was based primarily on analysis of the videos, as the coverage of the airgap probes was not sufficient to capture the worst events. The current deck height of 45 ft above MWL is sufficient to withstand the specified extreme event. Additional tests are planned to determine the response in sea-states with larger significant wave height and longer peak periods.

CONCLUDING REMARKS

The response of a minimal floating platform composed of three rectangular columns, and a large horizontal water-entrapment plate at the keel was determined experimentally, and a "semi-empirical" numerical algorithm was developed to predict the platform response. The hydrodynamic problem is deemed too complex for computational fluid dynamics, as the flow is three-dimensional, and viscous effects, as well as wave radiation and diffraction effects are significant.

The semi-empirical model is based on an extension of the Morison equation applied to members located at the edges of the plate and subject to normal loads only, with the relative velocity between the fluid and the members being computed from the undisturbed wave kinematics, and rigid body motion. Drag coefficients were determined based on experimental decay tests.

Laboratory tests were conducted at the U.C. Berkeley Ship Model Testing Facility to establish the validity of the numerical approach. Challenges of testing a deepwater platform in a relatively small wave basin were presented. Meaningful results could be obtained by performing a series of additional test aimed at independently validating every element of the numerical model.

The model test results confirmed the importance of a model capable of computing viscous effects generated by the

Copyright © 2005 by ASME

wave kinematics, as they do impact substantially the platform response. Optimizations of the shape of the water-entrapment plate are currently being conducted to further reduce wave-induced motion of the platform, These could not be completed meaningfully until the validity of the numerical algorithm had been established.

Some adjustments to the model are required to capture more precisely the slow drift response. These could be empirical using directly the model test results, or semi-empirical based on a numerical prediction of wave run-up and high order diffraction forces on the columns.

ACKNOWLEDGMENTS

The author wish to acknowledge the collaboration of Prof. R.W. Yeung in arranging use of the U.C. Berkeley Ship Model Testing Facility for this Research & Development project.

REFERENCES

[1] Cermelli, C.A., Roddier D.G., Busso C.C. (2004) *MINIFLOAT: A novel concept of minimal floating platform for marginal field development.* In Proc. Int. Offsh. And Polar Engrg Conf., Toulon, France

[2] Chen H.C., Liu T., and Huang E.T. (2002) *Time-Domain Simulation of Barge Capsizing by a Chimera Domain Decomposition Approach.* In Proc. Twelfth Int. Offsh. and Polar Eng. Conf., Kitakyushu, Japan

[3] Forristall, G.Z. (1999) *Wave crest distribution: observations and second order theory.* In Journal of Physical Oceanography, Vol. 30, p. 1931-1943

[4] Lake, M., He. H., Troesch A.W., Perlin, M., and Thiagarajan, K.P. (1999) *Hydrodynamic coefficient estimation for TLP and spar structures.* In Proc. 17th Int. Conf. on Offsh. Mech. and Arctic Engrg, Newfoundland, Canada

[5] Newman, J.N. (1974) *Second-order, slowly-varying forces on vessels in irregular waves.* In Proc. of the Symp. on the Dynamics of Marine Vehicles and Structures in Waves, London, 182-186.

[6] Newman, J.N. (1977) *Marine Hydrodynamics*, MIT Press

[7] Prislin, I., Blevins, R.D., Halkyard, J.E. (1998) *Viscous damping and added-mass of solid square plates.* In Proc. 17th Int. Conf. on Offsh. Mech. and Arctic Engrg

[8] Trulsen, K. and Teigen, P. (2002) *Wave scattering around a vertical cylinder: fully nonlinear potential flow calculations compared with low order perturbation results and experiment.* In Proc. 21st Int. Conf. on Offsh. Mech. and Arctic Engrg, Oslo, Norway

[9] Wheeler, J.D. (1969). *Method of calculating forces produced by irregular waves*. In Proc. First Offsh. Tech. Conf, OTC 1006, Houston

[10] Yeung R.W., D. Roddier, B. Alessandrini, L. Gentaz and S.-W. Liao, (2000) *Hydrodynamics of Rectangular Cylinders fitted with Bilge Keels in Roll Motion* 23rd ONR Symposium on Naval Hydrodynamics, France.

Copyright © 2005 by ASME

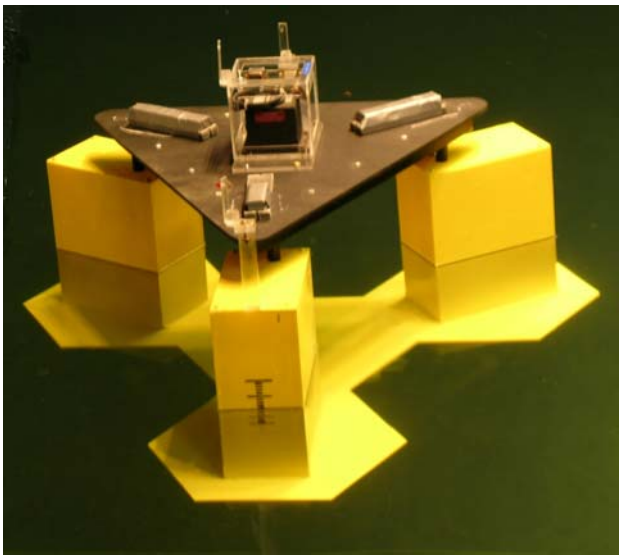

Figure 1a: 1/76 scale model of MINIFLOAT platform at the U.C. Berkeley Ship Model Testing Facility.

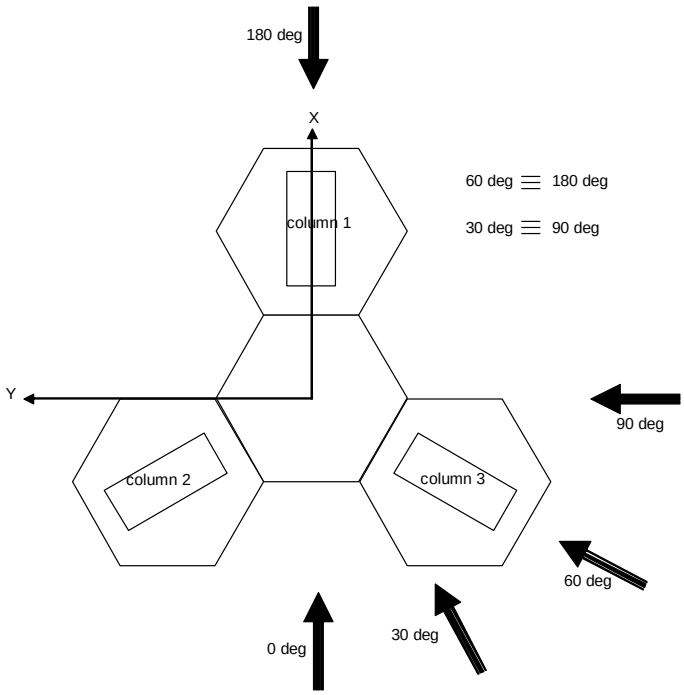

Figure 1b: Definition of wave heading with respect to platform. Because of symmetries, 0 deg, 90 deg and 180 deg headings correspond to headings every 30 degrees around the platform.

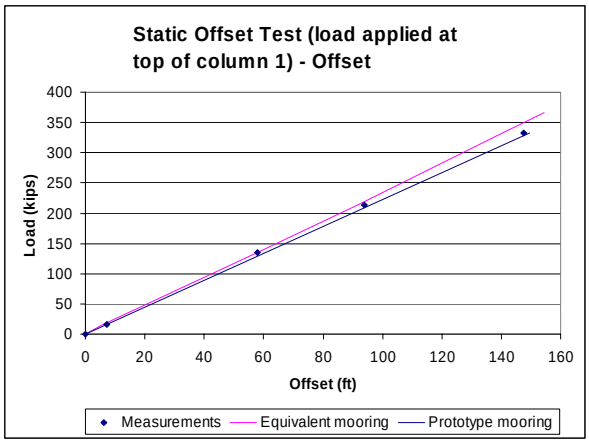

Figure 2a: Horizontal stiffness of prototype, and equivalent mooring system.

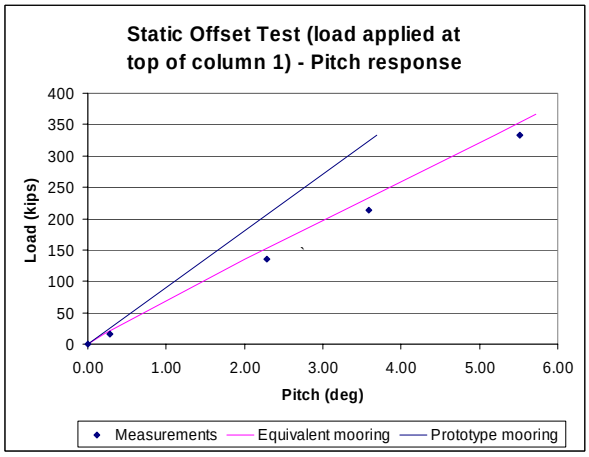

Figure 2b: Tilt angle due to moment applied in static offset test.

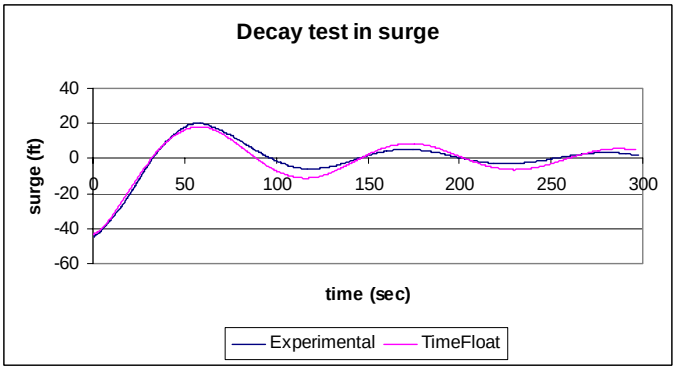

Figure 3a: Surge decay test – Experimental results and numerical simulations with adjusted drag coefficients on columns.

Copyright © 2005 by ASME

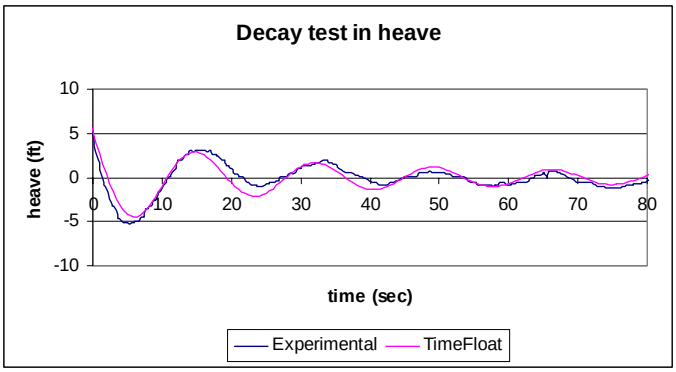

Figure 3b: Heave decay test – Experimental results and numerical simulations with adjusted drag coefficients on edges of water-entrapment plate.

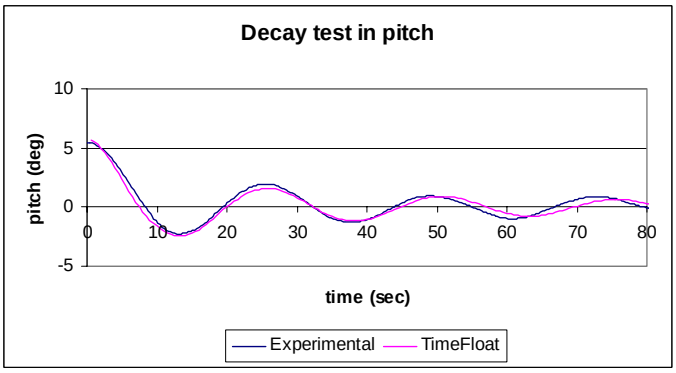

Figure 3c: Pitch decay test – Experimental results and numerical simulations with drag coefficients obtained from surge and heave decay tests.

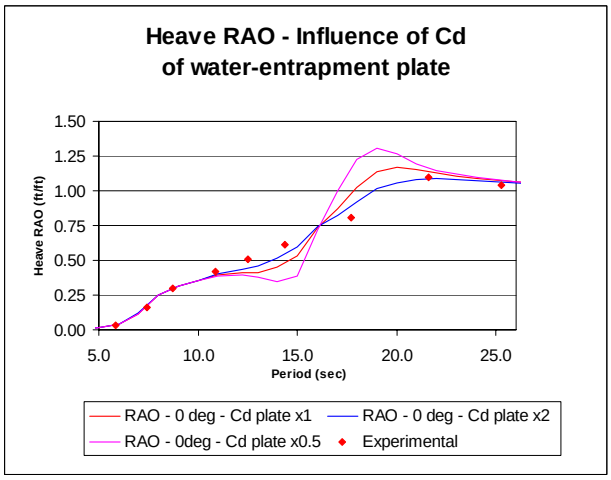

Figure 4a: Heave RAO at 0 deg heading. Comparison with numerical simulations with base case drag coefficients on the edges of the plate obtained from heave decay test, and sensitivity with drag coefficients that are twice bigger, and twice smaller than in the base case.

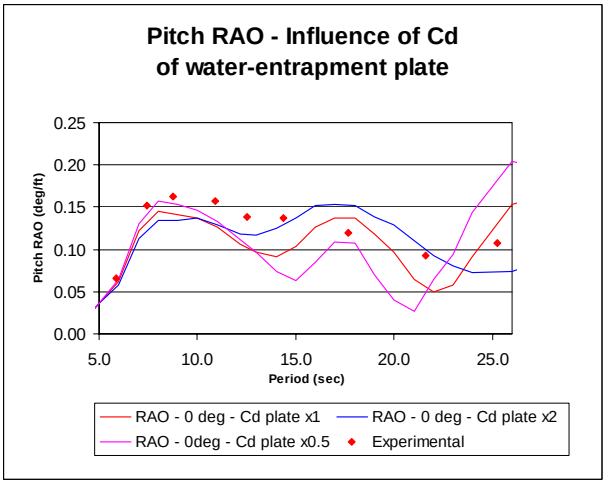

Figure 4b: Pitch RAO at 0 deg heading. Comparison with numerical simulations, and sensitivity with drag coefficients that are twice bigger, and twice smaller than in the base case.

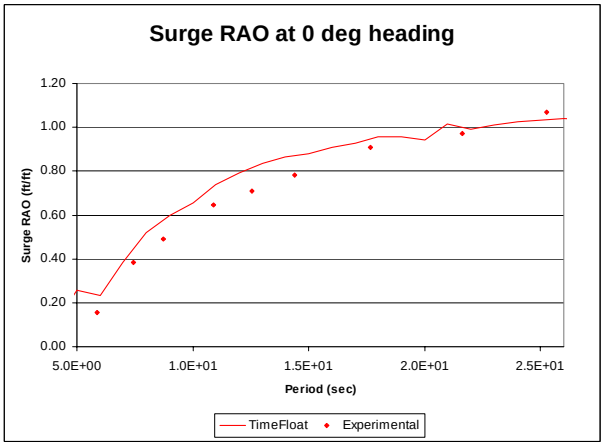

Figure 4c: Surge RAO at 0 deg heading and comparison with numerical simulations.

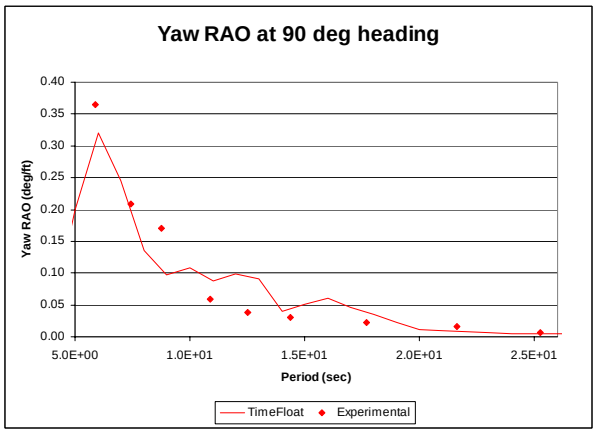

Figure 4d: Yaw RAO at 90 deg heading and comparison with numerical simulations.

Copyright © 2005 by ASME

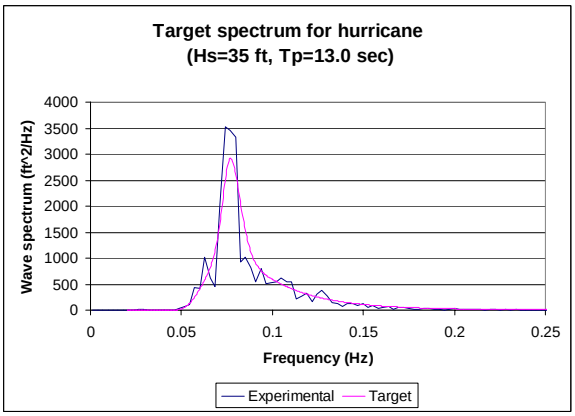

Figure 5a: Target wave spectrum and measured wave spectrum for 35 ft Hs, 13 sec. Tp Jonswap spectrum with gamma factor=3.

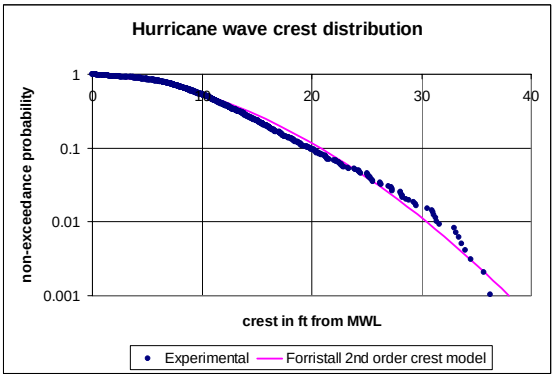

Figure 5b: Wave crest distribution in hurricane sea-state from measurements and comparison with Forristall's second order crest model.

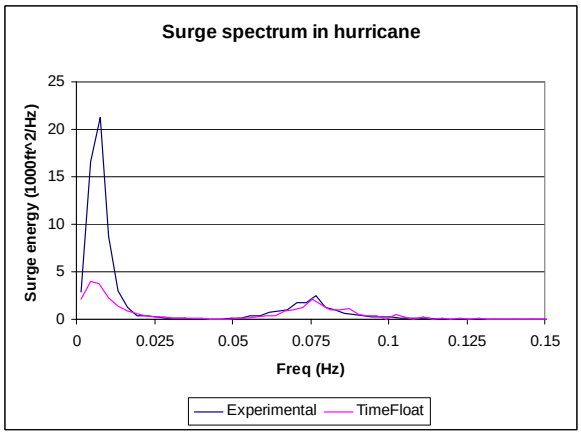

Figure 6a: Spectrum of surge response in hurricane. Experimental results and numerical predictions.

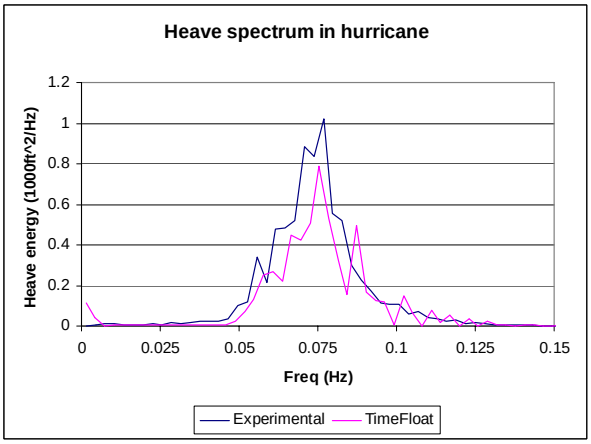

Figure 6b: Spectrum of heave response in hurricane. Experimental results and numerical predictions.

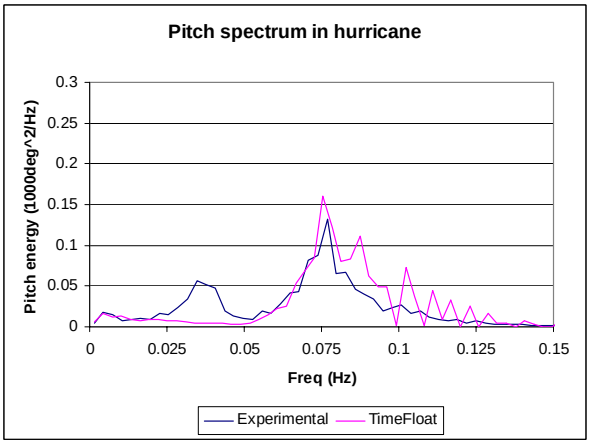

Figure 6c: Spectrum of pitch response in hurricane. Experimental results and numerical predictions.

Copyright © 2005 by ASME